Radiation induced acceleration of ions

Evgeny Gelfer[1,2,*], Alexander Fedotov[2], and Stefan Weber[1,3]

[1]ELI-Beamlines, Institute of Physics of the Czech Academy of Sciences, Dolni Brezany, 252 41 Czech Republic
[2]National Research Nuclear University MEPhI (Moscow Engineering Physics Institute), Moscow, 115409 Russia
[3]School of Science, Xi'an Jiaotong University, Xi'an 710049, China
[*]Corresponding author. Email: egelfer@gmail.com

arXiv:1907.02621v1 [physics.plasm-ph] 4 Jul 2019

ABSTRACT

In a transparent target exposed to a strong laser pulse radiation friction can have a substantial impact on electron dynamics. In particular, by modifying quiver electron motion, it can strongly enhance the longitudinal charge separation field, thus stimulating ion acceleration. We present a model and simulation results for such a radiation induced ion acceleration and study the scaling of the maximal attainable ion energy with respect to the laser and target parameters. We also compare the performance of this mechanism to the conventional ones.

Introduction

A new generation of 10 PW laser facilities is now under construction in Europe,[1–3] and even more powerful $100 \div 200$ PW projects are announced[4,5]. These lasers will generate pulses with intensities in the range $10^{23} - 10^{24}$ W/cm^2. Electron motion in such an intense field is strongly affected by radiation friction[6–8] (RF), which was recently directly observed in the experiments on head on collision of intense laser pulses with energetic electrons[9,10] and ultrarelativistic positron propagation in silicon[11].

A promising application of the powerful lasers is ion acceleration in a plasma. Note that in contrast to laser electron acceleration, where a great progress is observed even with the existing lasers and reaching 8 GeV energy level has been recently reported[12], energies of laser accelerated ions in experiments have not yet reached the level of 100 MeV[13,14]. Though it is already enough for such applications as proton radiography[15,16] or materials stress testing[17], some others, including hadron therapy for cancer treatment[18,19] or fast ignition of nuclear fusion[20], require higher ion energy[16,21,22].

A number of mechanisms for laser ion acceleration in a plasma are known. In the context of high power lasers the radiation pressure acceleration[20,23–32] (RPA) attracts the most attention due to a strong (linear) scaling of the ions energy with laser intensity. Irrespectively to that the details are peculiar to the cases of thin[24–30] and thick[20,23,31,32] target (called the light sail (LS) and hole boring (HB) regimes, respectively), the main idea of this scheme is the following: while a strong laser pulse is reflected from a dense plasma target, it pushes the plasma electrons forward, thus creating a charge separation longitudinal electric field, which in turn accelerates the ions. It should be stressed that, in spite of notable activity, the currently known results on the impact of RF on RPA remain controversial and fragmentary. It was shown[33–35] that RF has a limited impact on ion acceleration in the LS regime. This looks natural, as due to the target opacity only a minority of electrons may appear in a strong field region experiencing the RF force. However[36], RF can noticeably reduce ions energy in the HB case. In contrast, in a transparent target[37,38] RF can substantially affect the laser-plasma dynamics. Though it was demonstrated by PIC simulations that it can enhance ion acceleration[36,39], no quantitative theoretical model was provided.

Recently we discovered analytically and numerically[40,41] that by modifying the transverse quiver electron motion[42–44], and hence the longitudinal component of the $\mathbf{v} \times \mathbf{B}$ Lorentz force acting on electron, RF can enhance the efficiency of charge separation in a transparent plasma. Here we show how this effect can be applied for ion acceleration. We consider an intense laser pulse, incident normally on a thin transparent foil, with RF taken into account, and develop a 1D model capable for estimating the energy of accelerated ions for given laser and target parameters. We justify our model by PIC simulations and demonstrate that such radiation induced acceleration (RIA) mechanism can produce ions with considerably higher energy than RPA.

Results

On touching a target, a laser pulse of ultrarelativistic intensity pushes the electrons forward, instantly accelerating them almost to the speed of light. Snapshots from a typical 1D PIC simulation of a pulse incidence on an underdense plasma foil, with and without RF taken into account, are presented in Fig. 1. One can observe that with RF taken into account much more electrons are captured accelerating inside the laser pulse. As a consequence, the longitudinal charge separation field, the maximal energy, and the number of accelerated ions in Fig. 1(a) (for the latter see also Fig. 2) are also much higher than in Fig. 1(b).

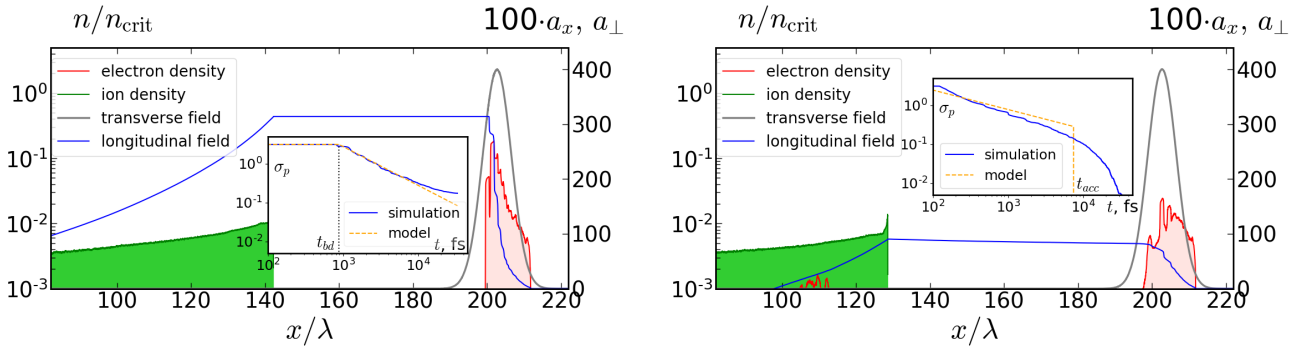

Figure 1. Particle densities and field distributions from 1D PIC simulations with (a) and without (b) RF at $t = 600$ fs. Insets: electron charge captured inside the pulse σ_p vs time. Laser parameters: field strength $a_0 = 400$ ($I = 4.4 \cdot 10^{23}$ W/cm^2), FWHM pulse duration 30 fs, circular polarization. Target density $n = 0.5 n_c$ and thickness $d = \lambda = 1\mu$m.

The inset in Fig. 1(a) shows that, with RF taken into account, the acceleration process splits into two stages. On the initial stage the charge captured inside the pulse is conserved, meaning that all the electrons from the target are moving inside the laser pulse. However, since they are slower than the pulse, they gradually drift from its front to back. Eventually, at some moment $\tau_{\rm bd}$ when the electrons reach the region where the laser field is not strong enough to balance the electrostatic field, a breakdown occurs[40,41]. On the second stage the electron liquid leaks away from the back of the pulse, and the ion acceleration saturates. Let us call this regime the radiation induced acceleration (RIA). According to the model developed in Methods, the time dependence of the maximal energy of the ions on each stage can be estimated as

$$\mathscr{E}^{(\rm RIA)}_{i,\max}(\tau) \sim \begin{cases} m_e \sigma_0 \tau, & \tau < \tau_{\rm bd}, \\ \frac{1}{2} m_e \mu a_0^4 T \left(1 + \ln \frac{\tau}{\tau_{\rm bd}}\right), & \tau > \tau_{\rm bd}, \end{cases} \tag{1}$$

where the constant $\mu = 1.18 \cdot 10^{-8}$ characterizes RF, $a_0 = eE_0/m_e\omega$ is the dimensionless field strength amplitude, m_e and $-e$ are electron mass and charge, $\sigma_0 = \tilde{n}_0 \omega d$ is the dimensionless areal density of the target, $\tilde{n}_0$ and d are its density (in the units of critical density $n_c = m_e\omega^2/4\pi e^2$) and thickness, respectively, τ and T are time and pulse duration measured in units of ω^{-1} and we assume the units are such that $c = 1$. The breakdown time is estimated as (see Methods)

$$\tau_{\rm bd} \approx \frac{\mu a_0^4 T}{2\sigma_0}. \tag{2}$$

If RF is neglected, then a charge separation required for ion acceleration is provided by the ponderomotive force. Let us call this regime the ponderomotive acceleration (PA). In this case, the charge captured inside the pulse is decreasing from the very beginning, meaning that a breakdown occurs almost immediately, see the inset in Fig. 1(b). The maximal energy of the ions can be estimated as (see Methods)

$$\mathscr{E}^{(\rm PA)}_{i,\max}(\tau < \tau_{\rm acc}) \sim m_e a_0 \sqrt{\frac{\tau}{T}}. \tag{3}$$

This estimation is valid until all the electrons leave the laser pulse. At that moment $\tau_{\rm acc} = CT$ the ion acceleration terminates, hence the maximal final ion energy is given by

$$\mathscr{E}^{(\rm PA)}_{i,\max}(\tau > \tau_{\rm acc}) \sim m_e a_0 \sqrt{C}. \tag{4}$$

The value of the constant factor $C \approx 400$ is determined from simulations. Note that it depends on the shape of the temporal envelope of the pulse, and that the given value is obtained for the Gaussian one.

As shown in Fig. 2, the resulting estimations (3) and (4) are in good agreement with 1D PIC simulations, especially for CP laser pulses. The results for linear polarization (LP) can be obtained by a substitution[41] $a_0 \to a_0/\sqrt{2}$. One can also see that for strong ($I \gtrsim 10^{23}$ W/cm^2) laser pulses RIA is much more efficient than PA due to a stronger scaling with a_0. This is in agreement with the condition

$$\mu a_0^3 T \gtrsim 1, \tag{5}$$

following from comparing the final maximal energies (3) and (4) predicted by our model. Note that precisely the same criterion arised in a problem of charge separation in a plasma with immobile ions[40,41].

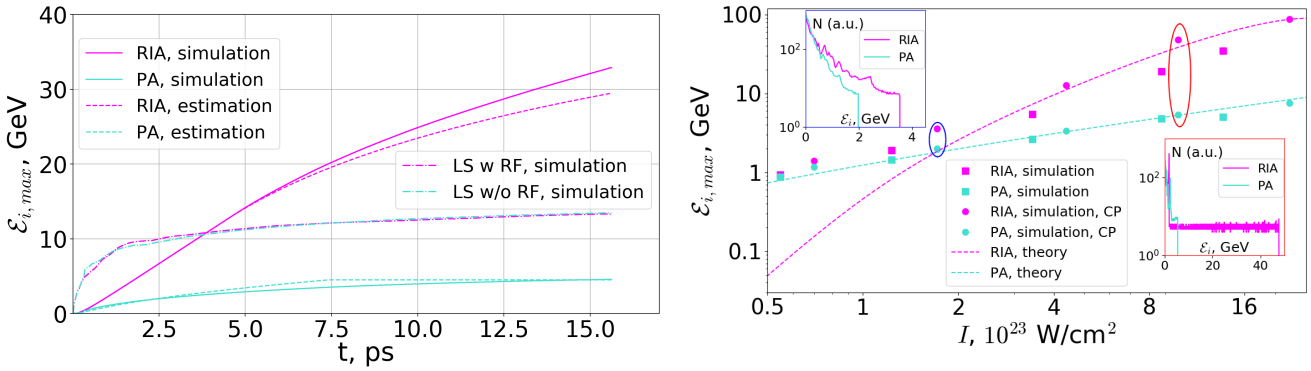

Figure 2. Maximal ion energies from 1D numerical simulations for different acceleration mechanisms. Left: maximal ion energy vs. time for a CP laser pulse with $a_0 = 600$ ($I \approx 10^{24}$ W/cm^2), target density: $n = 0.5n_c$ for RIA / PA, and $n = 190n_c$ for LS. Right: maximal ion energy at $t = 30$ ps vs. laser intensity for $n = 0.5n_c$. Insets: ion spectra for $a_0 = 250$ ($I \approx 1.7 \cdot 10^{23}$ W/cm^2) and $a_0 = 600$ ($I \approx 10^{24}$ W/cm^2).

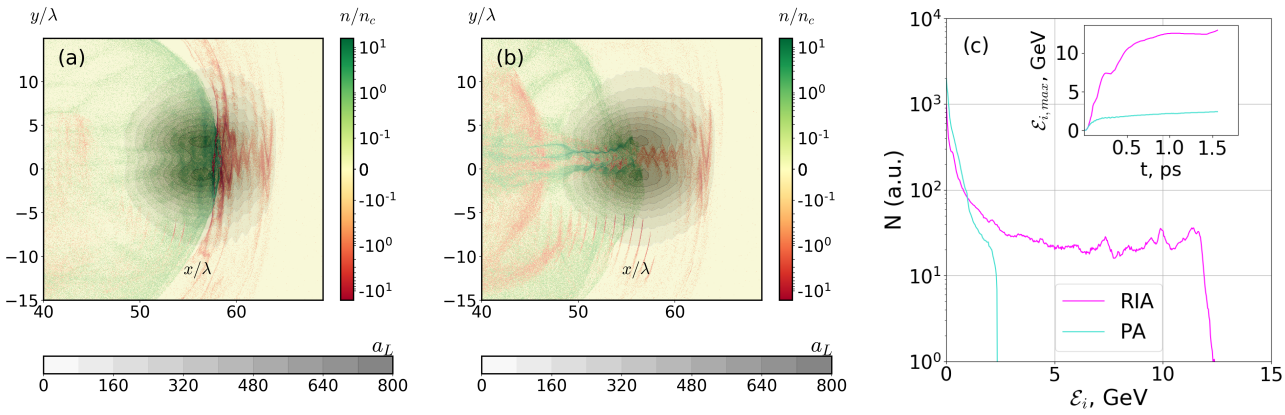

Figure 3. 2D PIC simulation results for ion acceleration in a transparent target: charge density (color scale) and laser field (grey scale) distributions at $t = 110$ fs with (a) and without (b) RF; (c) – ion spectra for RIA and PA at $t = 1480$ fs; inset: maximal ion energy for RIA and PA vs time. Laser pulse parameters: $I = 1.3 \cdot 10^{24}$ W/cm^2, FWHM pulse duration 30 fs, waist radius $w = 6\lambda$, circular polarization; target density $n_0 = 16n_c$ and thickness $d = \lambda$.

Discussion

We examined the impact of RF on ion acceleration by strong laser pulses in a thin transparent plasma target. For each of the alternative acceleration mechanisms (RIA and PA, based on pushing the electrons forward either by the RF induced longitudinal Lorentz force, or by the ponderomotive force, respectively), we elaborated a proper 1D analytical model. As shown in Fig. 2, each model is in excellent agreement with 1D PIC simulations. By using either Eqs. (3) and (4) or 1D PIC simulations, we identified the parameter regions where RF essentially enhances ion acceleration. Moreover, it can even outperform (in terms of the maximal ion energy) LS, commonly accepted as favorable for intense lasers and almost unaffected by RF[33], see Fig. 2(a).

Let us discuss this point in more detail. According to a convential 1D model for LS acceleration[24], the energy of the laser pulse is almost entirely converted into the energy of the ions. By taking into account that the optimal foil areal density for LS is

$\sigma_0 \sim a_0$[25], this is equivalent to the scaling

$$\mathscr{E}_i^{(\mathrm{LS})} \sim m_e \frac{a_0^2 T}{\sigma_0} \sim m_e a_0 T. \tag{6}$$

Then, by comparing Eq. (6) to Eq. (1), we conclude that RIA can outperform LS for $\mu a_0^3 \gtrsim 1$, i.e. for $a_0 \gtrsim 500$. Note that, in contrast to LS, in the RIA case only a small fraction of laser energy is transferred to particles (as is seen, e.g., from that the Gaussian laser profile in Fig 1(a) remains undistorted). Nevertheless, being distributed among much fewer number of particles (as compared to LS), this can still provide higher energy for the fastest ones.

In order to test RIA under more realistic conditions, we also made 2D simulations with a focused laser pulse, see Fig. 3. Here the ponderomotive force expels the electrons in transverse direction, thus reducing the charge separation field[40], see Fig. 3(a,b). Besides, the laser field amplitude reduces with time due to diffraction of the pulse. These negative for RIA effects are partially compensated by opting the value of the target charge areal density σ_0 higher than in 1D case. This reduces the breakdown time τ_{bd} with respect to the transverse expansion and laser diffraction times. As a result, RF still allows more electrons to propagate inside the pulse (compare Figs. 3(a) and (b)), thus increasing the ions energy, as well as the total number of accelerated ions, see Fig. 3(c). However, the estimation (1) is no more accurate quantitatively and should be refined by taking a proper account for the 2D effects. This is a hard separate problem still to be solved.

Methods

Analytical model

In order to study the ion motion, let us assume that the target is initially so thin, that for a time being the majority of electrons is moving inside the laser pulse, remaining completely separated from the ions accelerating behind the pulse (see Fig. 1) and generalize the model developed in Refs.[40,41] accordingly. Such electrons can be described by a hydrodynamic version of Eq. (2) from Ref.[40]:

$$\frac{\partial u_x}{\partial \tau} + v_x \frac{\partial u_x}{\partial \xi} = \frac{1}{2\gamma}\frac{da^2}{d\varphi} + \mu a^4 \frac{1-v_x}{1+v_x} - \sigma. \tag{7}$$

Here $\mathbf{u}(\tau,\xi) = \mathbf{p}/m$ is dimensionless momentum of the electrons at a fixed location, $\gamma = \sqrt{1+u^2}$, $v_x = u_x/\gamma$, $\tau = \omega t$, $\xi = \omega x$, $\mu = 2\omega r_e/3 \simeq 1.18 \cdot 10^{-8}$, $r_e = e^2/m$ – classical electron radius (we use the units with light speed $c = 1$), m_e and $-e$ are the electron mass and charge. Unless stated the opposite, we assume that the laser field is circularly polarized (CP), so that its dimensionless amplitude can be expressed as $\boldsymbol{a}_\perp \equiv e\mathbf{E}/m\omega = a(\varphi)\{0, \cos\varphi, \sin\varphi\}$, where $\varphi = \omega(t - x/c)$ is the phase. In 1D the longitudinal charge separation field coincides with the amount of charge $\sigma(\tau,\xi) = \int_\xi^\infty \tilde{n}(\xi')d\xi'$ located after ξ towards the laser propagation direction, where $\tilde{n} = n/n_c$ and $n_c = m_e\omega^2/4\pi e^2$ is the plasma critical density. Assuming that the longitudinal electron motion is ultrarelativistic ($\gamma \approx u_x \gg u_\perp \approx a$) and appending the continuity equation, we have

$$\frac{\partial u_x}{\partial \tau} - \frac{\partial}{\partial \varphi}\left(\frac{a^2}{2u_x}\right) - \frac{\mu a^6}{4u_x^2} + \sigma = 0, \quad \frac{\partial \sigma}{\partial \tau} + \frac{\partial \sigma}{\partial \varphi}\frac{a^2}{2u_x^2} = 0. \tag{8}$$

Under the above assumptions ion acceleration is governed by the total electron charge $\sigma_p(\tau) = \sigma(\tau, \varphi = T) = \int_{-\infty}^{T} \tilde{n}(\tau,\varphi')d\varphi'$ captured inside the laser pulse, where T is the dimensionless pulse duration. Indeed, the maximal longitudinal momentum and energy of the ions are expressed by

$$u_{i,\max}(\tau) = \frac{m_e}{m_i}\int_0^\tau \sigma_p(\tau')d\tau', \quad \mathscr{E}_{i,\max} = m_i\sqrt{1+u_{i,\max}^2}, \tag{9}$$

where m_i is the ion mass. As for the characteristic times τ_{bd} and τ_{acc}, they are determined by the motion of leftmost and rightmost electrons, respectively.

To find the accelerating field $\sigma_p(\tau)$, let us consider separately the two concurring mechanisms of charge separation in a transparent thin foil[40,41], RIA and PA. In the RIA case we neglect the second term in the first of Eqs. (8) and estimate the longitudinal 4-velocity of electrons inside the pulse by balancing the terms corresponding to the electrostatic force and the RF induced longitudinal Lorentz force:

$$u_x \sim \frac{a^3}{2}\sqrt{\frac{\mu}{\sigma}}. \tag{10}$$

For $\tau < \tau_{\rm bd}$ the value of $\sigma(\tau,\varphi)$ at the position of the leftmost electron inside the pulse is equal to σ_0. The breakdown time (2) is obtained from the condition $\int_0^{\tau_{\rm bd}}(1-v_x)d\tau \sim T$, where $v_x \approx 1 - a^2/2u_x^2$ is the velocity of the leftmost electron. The meaning of this condition is precisely that a breakdown occurs when the leftmost electrons have passed to the back of the pulse.

For $\tau > \tau_{\rm bd}$ the charge inside the pulse can be calculated by incorporating Eq. (10) into the continuity equation:

$$\frac{\partial\sigma}{\partial\tau} + \frac{\partial\sigma}{\partial\varphi}\frac{2\sigma}{\mu a^4} = 0. \tag{11}$$

After separating the variables in Eq. (11) we obtain the solution

$$\sigma \approx \frac{\mu}{2\tau}\int a^4 d\varphi. \tag{12}$$

Estimating $\int_{-\infty}^{T} a^4 d\varphi \sim a_0^4 T$, we arrive at the expression for a charge captured inside the laser pulse

$$\sigma_p^{(\rm RIA)}(\tau) \sim \begin{cases} \sigma_0, & \tau < \tau_{\rm bd} \\ \mu a_0^4 T/2\tau, & \tau > \tau_{\rm bd} \end{cases}. \tag{13}$$

Recall our assumption that the laser pulse initially grabs all the electrons from the target, totally separating them from the ions. It means that while v_x is still small, the RF induced longitudinal force (the third term in Eq. (7)) should exceed the maximum possible charge separation force σ_0:

$$\mu a_0^4 > \sigma_0. \tag{14}$$

In the PA case we neglect the third term in the first of Eqs. (8) and assume that $a(\varphi) = a_0\alpha(\varphi/T)$, where the function $\alpha(\zeta)$ is such that: (i) it rapidly vanishes for $|\zeta| \gtrsim 1$, and (ii) $\alpha(0) = 1$. By seeking a solution of the resulting equations in the form $u_x = a_0\sqrt{\tau/T}\alpha^2(\varphi/T)/g(\varphi/T)$, $\sigma = a_0\nu(\varphi/T)/(2\sqrt{T\tau})$, they transform to

$$\nu = g' - \frac{\alpha^2}{g}, \quad \nu' g^2 - \alpha^2\nu = 0. \tag{15}$$

Since they no more contain large or small parameters, even without solving them we can claim that for an arbitrary pulse shape the charge captured inside the pulse can be estimated up to a numerical factor as

$$\sigma_p^{(\rm PA)}(\tau) \equiv \sigma(\tau,\varphi = T) \sim \frac{a_0}{2\sqrt{T\tau}}. \tag{16}$$

Estimations (13) and (16) are in a good agreement with simulations results, see the insets in Fig. 1. By substituting them into (9) in the ultrarelativistic limit $u_i \gg 1$ we arrive at (1) and (3), respectively.

To find the acceleration time $\tau_{\rm acc}$, we need to consider the motion of the rightmost electrons. Since at their location the field of the ions is screened almost completely, their equation of motion takes the form

$$\frac{du_{r,x}}{d\tau} = \frac{1}{2u_{r,x}}\frac{da^2}{d\varphi} + \frac{\mu a^6}{2u_{r,x}^2}. \tag{17}$$

Estimating $da^2/d\varphi \sim a_0^2/T$ and neglecting either the second or the first term on the right hand side, we obtain the solutions

$$u_{r,x}^{(\rm PA)} \sim a_0\sqrt{\frac{\tau}{T}}, \quad u_{r,x}^{(\rm RIA)} \sim a_0^2(\mu\tau)^{1/3} \tag{18}$$

for each case of PA and RIA, respectively. Now the acceleration time can be estimated from the condition $\int_0^{\tau_{\rm acc}} d\tau(1-v_{r,x}) \sim T$, where $v_{r,x}$ is the longitudinal velocity of the rightmost electrons. The meaning of this condition is that acceleration saturates when the rightmost electrons have passed to the back of the pulse. For the case of PA, if we neglect the time period of nonrelativistic electron longitudinal motion, i.e. when $u_{r,x} < a_0$, then this condition is reduced to $\int_T^{\tau_{\rm acc}} d\tau/2\tau \sim 1$. Therefore in this case we obtain

$$\tau_{\rm acc}^{(\rm PA)} = CT, \tag{19}$$

where C is a numerical constant, which depends on a temporal profile of the laser pulse and can be determined from a numerical solution of (17) or from PIC simulations. For RIA the acceleration time can be estimated along the same lines as

$$\tau_{\rm acc}^{\rm (RIA)} \sim \mu^2 T^3 a_0^6 \tag{20}$$

To justify the consistency of our analysis let us inspect the parameter range for which either one of the second or the third terms in the right hand side of Eq. (8) can be neglected. Using the same estimation $da^2/d\varphi \sim a_0^2/T$ as above, we can see that the RF induced term dominates over the ponderomotive term if

$$\mu\sigma_0 a_0^2 T^2 > 1. \tag{21}$$

Note that under this condition also $\tau_{\rm acc}^{\rm (RIA)} > \tau_{\rm bd}$, justifying the appearance of the second stage of RIA described by the second line of Eq. (1). Finally we note that the obtained conditions (14) and (21) jointly establish an existence domain for RIA, which is non-empty under the condition (5). These conditions are extremely useful for selecting the parameters for both 1D and 2D simulations.

Numerical approach

For numerical simulations we used PIC code SMILEI[45], which allows to make calculations with and without RF taken into account. In all simulations we used laser pulses with the wavelength $\lambda = 1\mu$m and the Gaussian temporal profile $a(\varphi) = a_0 \exp[-(\varphi - 4T)^2/T^2]$. The dimensionless pulse duration T is related to FWHM duration by $T \approx 0.57\omega t_{\rm FWHM}$. For 2D simulations we used laser pulses with a supergaussian spatial profile, see[46] for the details of implementation of arbitrary pulse shapes in SMILEI. The intensity distribution in a focal plane was of the form $I \sim \exp[-(y/w)^8]$, where the laser pulse waist $w = 6\lambda$.

For 1D simulations we used 100 cells per wavelength and 200 particles of each type per cell for low density foils and 1000 particles per cell for high density ones; time step was equal to a space step divided by the factor $c/0.95$. 2D simulations were done inside a $500\lambda \times 128\lambda$ box with the cell side length $dx = dy = \lambda/100$ in both directions. Time step was chosen as $dt = 0.95dx/c\sqrt{2}$, and the number of particles of each type per cell was equal to 16. Target density for LS simulation satisfied the condition[25] $l/\lambda = a_0/\pi\tilde{n}$. Boundary conditions for particles and fields were absorptive. The target thickness was $d = \lambda$, and the laser was focused on its left boundary, located at $x = 30\lambda$.

Data Availability Statement

The datasets generated and analyzed in this research are available from the corresponding author upon a request.

Acknowledgements

We are grateful to S.V. Bulanov, S.S. Bulanov, O. Klimo, T. Schlegel, M. Vranic for valuable discussions, and to M. Grech for both valuable discussions and assistance with the code. The results of the project LQ1606 were obtained with the financial support of the Ministry of Education, Youth and Sports of the Czech Republic as part of targeted support from the National Programme of Sustainability II. The research was performed using the code SMILEI and the resources of the ELI Beamlines Eclipse cluster, and was partially supported by the projects ELITAS (ELI Tools for Advanced Simulation) CZ.02.1.01/0.0/0.0/16_013/0001793, ADONIS (Advanced research using high intensity laser produced photons and particles) CZ.02.1.01/0.0/0.0/16_019/0000789 and HiFI (High-Field Initiative) CZ.02.1.01/0.0/0.0/15003/0000449 from European Regional Development Fund, the MEPhI Academic Excellence Project (Contract No. 02.a03.21.0005), and the Russian Foundation for Basic Research (Grant 19-02-00643).

Author contributions

E.G., A.M. and S.W. proposed the idea of the research and reviewed the manuscript. E.G. and A.F. developed the analytical model. E.G. performed numerical simulations and wrote the manuscript.

Competing Interests

The authors declare that they have no competing interests.

References

1. http://www.eli-beams.eu
2. http://www.eli-np.ro/
3. http://portail.polytechnique.edu/luli/en/cilex-apollon/apollo
4. Cartlidge E. The light fantastic. *Science* **6374**, 382–385 (2018).
5. Bashinov A.V., Gonoskov A.A., Kim A.V., Mourou G., Sergeev A.M. New horizons for extreme light physics with mega-science project XCELS. *Eur. Phys. J. Spec. Top.* **223**, 1105 (2014).
6. Bulanov S.V., Esirkepov T. Zh., Koga J., and Tajima T. Interaction of electromagnetic waves with plasma in the radiation-dominated regime. *Plasma Physics Reports* **30**, 196 (2004).
7. Di Piazza A., Muller C., Hatsagortsyan K.Z., and Keitel C.H. Extremely high-intensity laser interactions with fundamental quantum systems. *Rev. Mod. Phys.* **84**, 1177 (2012).
8. Burton D.A. and Noble A. Aspects of electromagnetic radiation reaction in strong fields. *Contemp. Phys.* **55**, 110 (2014).
9. Cole J.M. et al. Experimental evidence of radiation reaction in the collision of a high-intensity laser pulse with a laser-wakefield accelerated electron beam. *Phys. Rev. X* **8**, 011020 (2018).
10. Poder K. et al. Experimental signatures of the quantum nature of radiation reaction in the field of an ultraintense laser. *Phys. Rev. X* **8** 031004 (2018).
11. Wistisen T.N., Di Piazza A., Knudsen H.V., and Uggerhoj U.I. Experimental evidence of quantum radiation reaction in aligned crystals. *Nature Comm.* **9**, 795 (2018).
12. Gonsalves A.J. et al. Petawatt Laser Guiding and Electron Beam Acceleration to 8 GeV in a Laser-Heated Capillary Discharge Waveguide. *Phys. Rev. Lett.* **122**, 084801 (2019).
13. Wagner, F. et al. Maximum Proton Energy above 85 MeV from the Relativistic Interaction of Laser Pulses with Micrometer Thick CH_2 Targets. *Phys. Rev. Lett.* **116**, 205002 (2016).
14. Higginson A. et al. Near-100 MeV protons via a laser-driven transparency-enhanced hybrid acceleration scheme. *Nature Comm.* **9**, 724 (2018).
15. Cobble J. A., Johnson R. P., Cowan T. E., Renard-Le Galloudec N., Allen M. High Resolution Laser-Driven Proton Radiography. *J. Appl. Phys.* **92**, 1775 (2002).
16. Borghesi M., Fuchs J., Bulanov S.V., Mackinnon A.J., Patel P.K., and Roth M. Fast Ion Generation by High-Intensity Laser Irradiation of Solid Targets and Applications. *Fusion Sci. Technol.* **49**, 412 (2006).
17. Barberio M. et al. Laser-accelerated particle beams for stress testing of materials. *Nat. Comm.* **9**, 372 (2018).
18. Bulanov S.V., Khoroshkov V.S. Feasibility of using laser ion accelerators in proton therapy. *Plasma Physics Reports* **28**, 453 (2002).
19. Bulanov S.V. et al. Laser ion acceleration for hadron therapy. *Phys.-Usp.* **57**, 1149 (2014).
20. Naumova N., Schlegel T., Tikhonchuk V.T., Labaune C., Sokolov I.V., Mourou G. Hole Boring in a DT Pellet and Fast-Ion Ignition with Ultraintense Laser Pulses. *Phys. Rev. Lett.* **102**, 025002 (2009).
21. Daido H., Nishiuchi M. and Pirozhkov A.S. Review of laser-driven ion sources and their applications. *Rep. Prog. Phys.* **75**, 056401 (2012).
22. Macchi A., Borghesi M., Passoni M. Ion acceleration by superintense laser-plasma interaction. *Rev. Mod. Phys.* **85**, 751–793 (2013).
23. Schlegel T., Naumova N., Tikhonchuk V.T., Labaune C., Sokolov I.V., and Mourou G. Relativistic laser piston model: Ponderomotive ion acceleration in dense plasmas using ultraintense laser pulses. *Physics of Plasmas* **16**, 083103 (2009).
24. Esirkepov T., Borghesi M., Bulanov S.V., Mourou G., Tajima T. Highly efficient relativistic-ion generation in the laser-piston regime. *Phys. Rev. Lett.* **92**, 175003 (2004).
25. Macchi A., Veghini S., Pegoraro F. "Light sail" acceleration reexamined. *Phys. Rev. Lett.* **103**, 085003 (2009).
26. Qiao B., Zepf M., Borghesi M., Geissler M. Stable GeV ion-beam acceleration from thin foils by circularly polarized laser pulses. *Phys. Rev. Lett.* **102**, 145002 (2009).
27. Bulanov S.V., Echkina E.Yu., Esirkepov T.Zh., Inovenkov I.N., Kando M., Pegoraro F., Korn G. Unlimited ion acceleration by radiation pressure. *Phys. Rev. Lett.* **104**, 135003 (2010).

28. Bulanov S.S. et al. Enhancement of maximum attainable ion energy in the radiation pressure acceleration regime using a guiding structure. *Phys. Rev. Lett.* **114**, 105003 (2015).

29. Bulanov S.S. et al. Radiation pressure acceleration: The factors limiting maximum attainable ion energy. *Phys. Plasmas* **23**, 056703 (2016).

30. Shen X.F. et al. Achieving stable radiation pressure acceleration of heavy ions via successive electron replenishment from ionization of a high-Z material coating. *Phys. Rev. Lett.* **118**, 204802 (2017).

31. Wilks S.C., Kruer W.L., Tabak M., Langdon A.B. Absorption of ultra-intense laser pulses. *Phys. Rev. Lett.* **69**, 1383–1386 (1992).

32. Psikal J., Matys M. Dominance of hole-boring radiation pressure acceleration regime with thin ribbon of ionized solid hydrogen. *PPCF* **60**, 044003 (2018).

33. Tamburini M., Pegoraro F., Di Piazza A., Keitel C.H., Macchi A. Radiation reaction effects on radiation pressure acceleration. *NJP* **12**, 123005 (2010).

34. Tamburini M., Pegoraro F., Di Piazza A., Keitel C. H., Liseykina T. V., Macchi, A. Radiation reaction effects on electron nonlinear dynamics and ion acceleration in laser–solid interaction. *Nucl. Instrum. A* **653**, 181-185 (2011).

35. Tamburini M., Liseykina T.V., Pegoraro F., Macchi A. Radiation-pressure-dominant acceleration: Polarization and radiation reaction effects and energy increase in three-dimensional simulations. *Phys. Rev. E* **85**, 016407 (2012).

36. Capdessus R. and McKenna P. Influence of radiation reaction force on ultraintense laser-driven ion acceleration. *Phys. Rev. E* **91**, 053105 (2015).

37. Vshivkov V.A., Naumova N.M., Pegoraro F., and Bulanov S.V. Nonlinear electrodynamics of the interaction of ultra-intense laser pulses with a thin foil. *Phys. Plasmas* **5**, 2727 (1998).

38. Gelfer E., Fedotov A., Klimo O., Weber S. Absorption and opacity threshold for a thin foil in a strong laser field. *arXiv: 1906.05902* (2019).

39. Chen M., Pukhov A., Yu T.-P., Sheng Z.-M. Radiation reaction effects on ion acceleration in laser foil interaction. *PPCF* **53**, 014004 (2011).

40. Gelfer E., Elkina N., Fedotov A. Unexpected impact of radiation friction: enhancing production of longitudinal plasma waves. *Sci. Rep.* **8**, 6478 (2018).

41. Gelfer E.G., Fedotov A.M., Weber S. Theory and simulations of radiation friction induced enhancement of laser-driven longitudinal fields. *PPCF* **60**, 064005 (2018).

42. Voronin B.S. and Kolomenskii A.A. The pressure of an intense plane wave on a free charge and on a charge in a magnetic field. *Sov. Phys. JETP* **65**, 1027–1031 (1965).

43. Zeldovich Ya.B. Interaction of free electrons with electromagnetic radiation. *Sov. Phys. Usp.* **18**, 79 (1975).

44. Di Piazza A. Exact solution of the Landau-Lifshitz equation in a plane wave. *Lett. Math. Phys.* **83**, 305 (2008).

45. Derouillat J. et al. SMILEI: a collaborative, open-source, multi-purpose particle-in-cell code for plasma simulation. *Comp. Phys. Comm.* **222**, 351–373 (2018).

46. Perez P. and Grech M. Oblique-incidence, arbitrary-profile wave injection for electromagnetic simulations. *Phys. Rev. E* 99, 033307 (2019).